Beilstein-Institut
Functional Nanoscience
May 17th – 21st, 2010, Bozen, Italy

Control of Rotary Motion at the Nanoscale: Motility, Actuation, Self-assembly

Petr Král*, Lela Vuković, Niladri Patra, Boyang Wang and Alexey Titov

Department of Chemistry, University of Illinois at Chicago, Chicago, IL 60607, U.S.A.

E-Mail: *pkral@uic.edu

Received: 21st September 2010 / Published: 13th June 2011

Abstract

Controlling motion of nanoscale systems is of fundamental importance for the development of many emerging nanotechnology areas. We review a variety of mechanisms that allow controlling rotary motion in nanoscale systems with numerous potential applications. The discussed mechanisms control molecular motors and propellers of liquids, nanoscale objects rolling on liquids, nanochannels with rotary switching motion and self-assembly of functional carbonaceous materials guided by water nanodroplets and carbon nanotubes.

Introduction

Today, manipulation of nanostructures in fluids is of great importance in nano- and biotechnology applications. Many examples of successful transport of nanoscale cargo in fluids can be found in biological systems. For example, cells can transport molecules and micelles [1] by kinesin [2], dynein [3] or myosin [4]. After picking up the cargo, these motor proteins can move along tubulous filaments. Other molecular motors can realize numerous types of motions [5], such as bacteria self-propelling by tiny flagella [6]. Controlled delivery of molecules and nanoscale objects *in vitro* can be realized by modifying existing natural

systems to perform desired transport tasks [7]. This approach has been successfully tested in microfluidic systems, where natural molecular motors were shown as good candidates for powering the transport of nanoparticles and other cargo [8 – 10].

Artificial molecular motors have been also synthesized [11]. They could be driven by optical [12 – 15], electrical [16], chemical [17], thermal [18], and other ratchet-like means [19, 20]. With the availability of nanoscale propelling units, the lab-on-a-chip concept [21] could be modified to study single molecules [22 – 24], and extended to another lab-in-a-cell concept, where individual biomolecules inside cells could be transported [25, 26].

Carbon-based materials with at least one spatial dimension at the nanoscale, such as carbon nanotubes, nanocones and graphene [27 – 29], have many unique properties that make them ideal for the fabrication of active nanofluidic elements. They are chemically stable, very strong and rigid, since covalent binding of their carbon atoms is realized by planar sp^2-orbitals. Carbon nanotubes (CNTs) can be modified by physisorption [30] or covalent bonding of molecular ligands [31]. The semi-metallic graphene could be also tuned by doping [32] and chemical functionalization [33 – 37]. The functionalized carbon nanostructures are promising building blocks of multi-component nanodevices, which could perform complex tasks. In this work, we explore potential nanotechnology and nanofluidics applications of these and other materials, including surfactant-covered metallic nanoparticles and hybrid (inorganic, organic, biomolecular) structures.

Control of Motility at the Nanoscale

In order to design autonomous nanoscale devices in liquids, we need to understand the physical laws which determine their motion. Flow of fluids around nanoscale structures is characterized by low Reynolds numbers (ratio of inertial and viscous forces), $R = a\nu\rho/\eta$, where a is the size of the system, ν its velocity, ρ its density and η is the viscosity of the fluid. In low-R environments, inertia is negligible, and viscosity dominates the motion of objects. According to "scallop theorem," systems can pump fluids and propel themselves in environments with low Reynolds numbers only if their motion is not time-reversible [38]. Unidirectional rotary motion is non-reversible and thus suitable for driving nanoscale processes in liquids.

Molecular propellers

Propellers are commonly used on macroscale to convert rotary motion into thrust. The performance of nanoscopic propellers with "chemically tunable" blades has been studied by molecular dynamics (MD) simulations [39]. The propellers are formed by (8,0) carbon nanotubes (CNT) [40], with chemically attached aromatic blades. These propellers could potentially be synthesized by cyclic addition reactions [41]. Two types of propellers were designed: (1) the bulk propeller, shown in Figure 1 (left), can pump liquid along the tube

z-axis, due to two blades being tilted with respect to the nanotube axis; (2) the surface propeller, shown in Figure 1, pumps water orthogonal to the tube axis by four larger blades aligned straight along the axis.

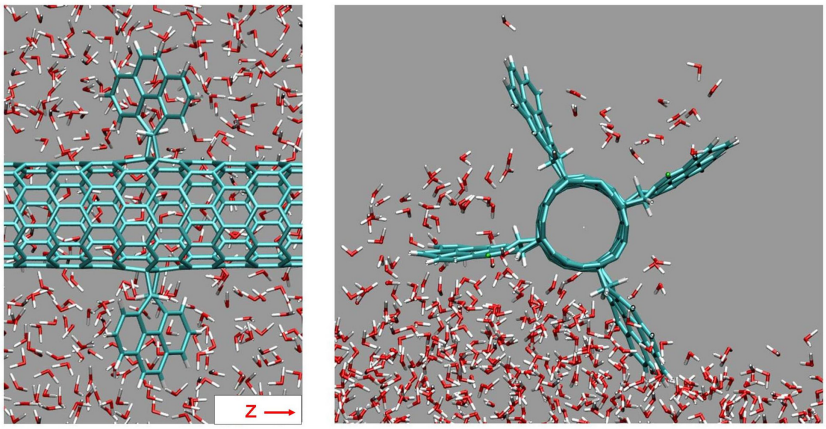

Figure 1. The bulk (left) and surface (right) water propellers that pump water along the tube (z) axis and orthogonal to it, respectively.

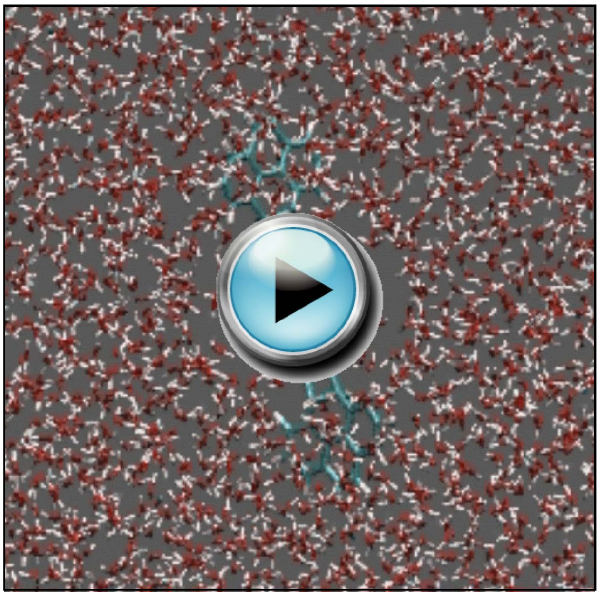

Movie 1. Hydrophic bulk propeller

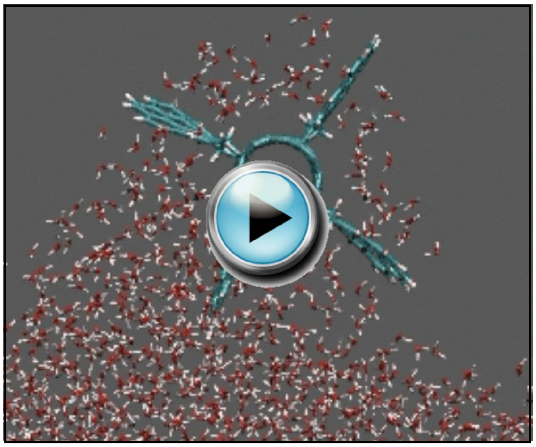

Movie 2. Hydrophilic surface propeller

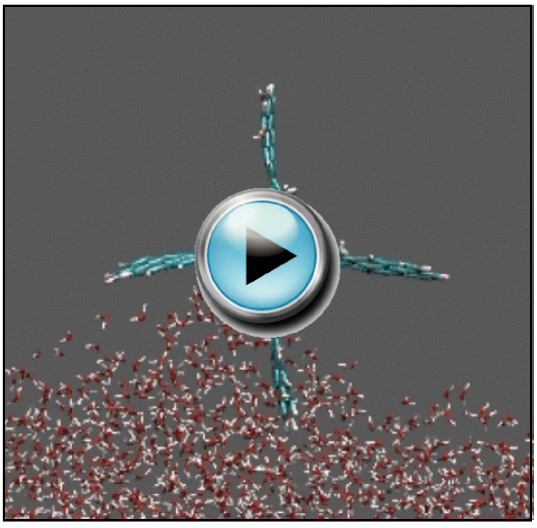

Movie 3. Hydrophobic surface propeller

Simulations have shown that these propellers can pump liquids when driven by constant applied torque on the CNT. Figure 2 shows the temperature dependence of the rotation rates (left) and pumping rates (right) of the bulk hydrophobic and hydrophilic propellers with different blades, obtained in the hydrophobic dichloromethane (DCM) and hydrophilic water solvents. As the system is heated above the (normal) freezing points of the solvents, $T^{DCM}_{f} = 175$ K and $T^{water}_{f} = 273$ K, the rotation rates grow, due to smaller solvent viscosities. The hydrophilic propeller rotates slower, since its polar blades interact stronger with both solvents. Substantially slower rotation occurs in water that forms hydrogen bonds with its polar blades [42] (see inset in Figure 2).

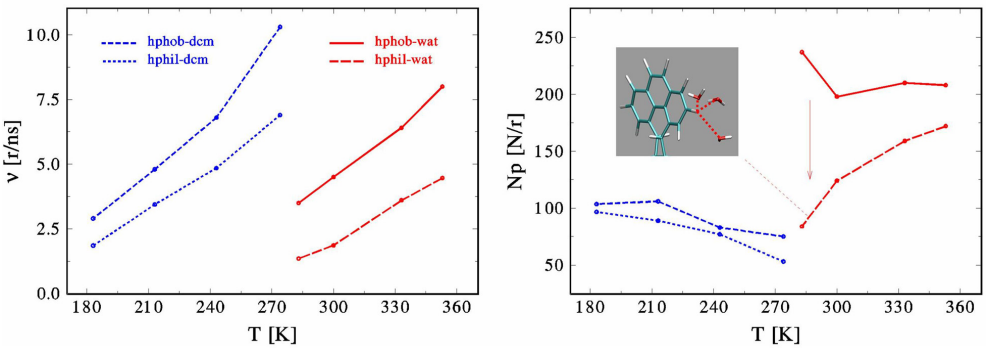

Figure 2. (left) Rotation rates (round/ns) of the bulk hydrophobic ("pho") and hydrophilic ("phi") propellers in water and DCM solvents as a function of temperature. (right) The pumping rates (molecules/round) of the bulk hydrophobic and hydrophilic propellers in water and DCM solvents as a function of temperature. (inset) Formation of hydrogen bonds between the hydrophilic blades and water can dramatically reduce the pumping rate.

The pumping rates are significantly different in two solvents, as seen in Figure 2 (right). In the DCM solvent, the pumping rates are low due to the weak coupling between the solvent molecules and the blades. Solvent molecules resemble ideal gas that "slips" on the blades in independent scattering events. The same is true for both hydrophobic and hydrophilic propellers, although in the hydrophilic case weak Coulombic coupling of the blades and DCM slightly slows down the pumping. At higher temperatures, momentum is dissipated faster and the pumping rate is reduced. In the polar (water) solvent, water molecules form clusters, around the blades, transiently held together by hydrogen bonds. This can effectively increase the cross section of the hydrophobic blades and the pumping rate, in agreement with Figure 2 (right). In the case of the hydrophilic propeller, water forms relatively stable hydration shells around the blades that reduce the effective space available for a direct contact of the pumped molecules with the blades. This causes drastically smaller pumping rates with respect to the hydrophobic propeller. At high temperatures, the hydrogen bonds break down and the pumping rates increase and tend to be the same in both types of propellers.

These molecular propellers could be used as functional components of nanomachines. One can imagine that a nanomotor (the gamma subunit of the F_1-ATPase enzyme), driven by the ATP hydrolysis, can be linked to the molecular propeller described above. In this way, a functional unit capable of transporting nanoscale cargo *in vitro* and *in vivo* could be obtained.

Molecular motors

Rotary motors could drive the above described molecular propellers. At the macroscale, electronic driving is the most efficient method of powering motors [43]. At the nanoscale, electronic driving could be achieved by *electron tunnelling*, which can induce periodic vibrational [44] and translational motion in molecules [45]. Here, we show how nanoscale vibrations can be effectively transformed into concerted rotary motion by electron tunnelling [46].

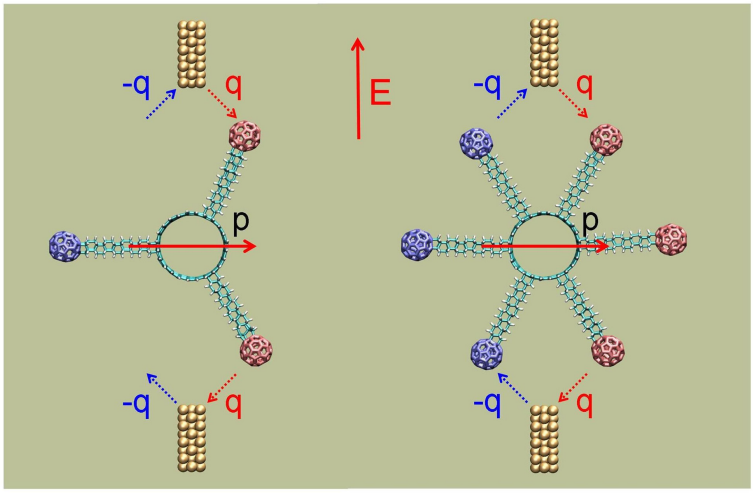

Figure 3. Tunneling-driven nanoscale motors with three (left) and six (right) fullerene blades. In an external homogeneous electric field E oriented along the vertical z direction, the electron tunneling from the neutral electrodes to the blades maintains an electric dipole p on the rotor, which is on average orthogonal to the field direction. This dipole is unidirectionally rotated by the electric field.

In Figure 3, we present two types of tunnelling-driven molecular motors, made with three (left) and six (right) stalks [46]. Their shaft is formed by a (12,0) carbon nanotube (CNT) [41], which could be mounted into CNT bearings [47]. The stalks, formed by polymerized iceane molecules with saturated bonds [48], are attached to the shaft at an angle of 120° or 60° with respect to each other. The length of stalks was chosen to prevent nonresonant electron tunnelling from the blades to the shaft [49]. The energies of their electronic states should also prevent the electron transfer along the stalks by resonant tunnelling [50]. The blades are made of molecules with conjugated bonds (fullerenes) covalently attached at the top of the stalks. A similar single molecule rotary motor based on a ruthenium complex was recently synthesized [51]. In our MD simulations, an external homogeneous electrostatic field ε, oriented along the vertical z direction, has been used for periodical charging and discharging of the blades by electron tunnelling from two neutral electrodes, placed and

immobilized in the proximity of the motor, as shown in the Figure 3. The field ε then powers the system by rotating the formed *dipole p* of the rotor that is on average orthogonal to the field direction.

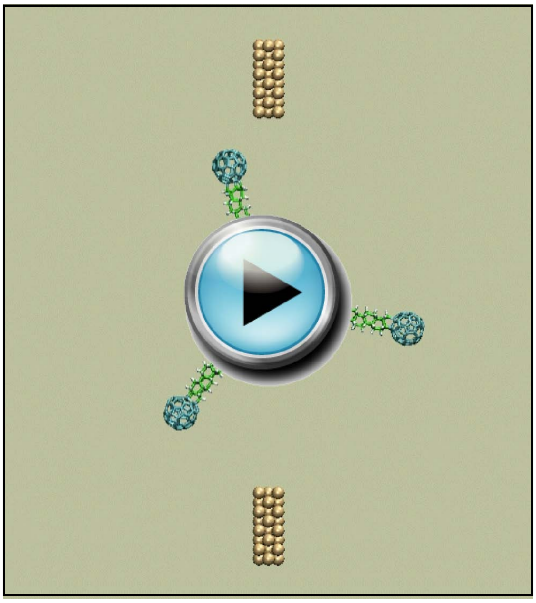

Movie 4. Rotary tunneling motor with 3 blades

In Figure 4, we show the efficiency of these tunnelling-driven motors obtained by applying a damping torque and stabilizing the motor rotation to the steady-state. In the limit of high damping torque (high loading), the efficiency saturates to the values of $\eta \approx 0.85$ and $\eta \approx 0.6$ for three- and six-fullerene motors, respectively. The maximum efficiency of the motors, $\eta = 1$, is never observed due to the dissipation of the torque to the internal damping phonon modes of the motor. For lower damping torques (low loading), the efficiency of these motors is vanishing, $\eta \rightarrow 0$, similar to the macroscopic electric motors [43]. These simulations demonstrate that rotary synthetic molecular motors can have robust performance under load, and in the presence of noise and defects.

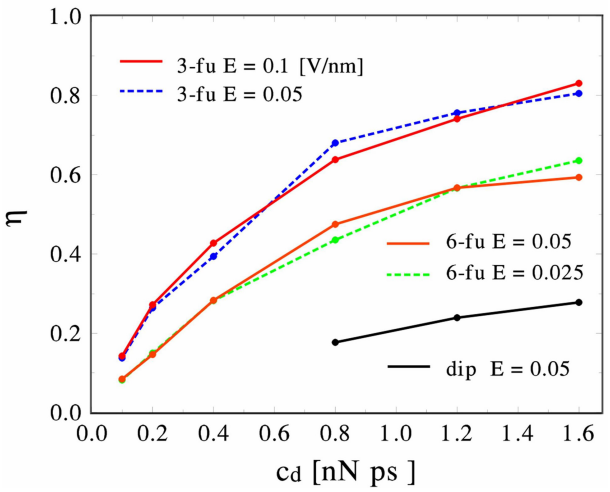

Figure 4. Dependence of the efficiency η for the 3-fullerene and 6-fullerene motors on the damping coefficient c_d. At larger c_d the efficiency grows and becomes stabilized, but $\eta_{3\text{-fu}} > \eta_{6\text{-fu}}$.

Molecular rollers

One can move nanoscale objects by AFM, light tweezers [52, 53] and other microscopic techniques. However, future nanosystems might need to move autonomously. Electrically, magnetically or optically active objects could be set in motion by the application of external fields. Nanoobjects responsive to external stimuli can be designed by appropriate chemistry.

Recently, this idea has been explored [54] by means of atomistic MD simulations, where surfactant-covered nanorods were rolled (and translated) on water surface when driven electrically. In Figure 5, we show a model of the alkane-covered nanorod, which has the empty coarse grained core that is locally and transiently charged on its surface. The driving of the model nanorods was simulated by adding small rechargeable electrodes on their surfaces: a narrow stripe of beads, positioned in the layer adjacent to the core and parallel to the water surface, is sequentially recharged (see Figure 5). We test two recharging regimes, where one stripe along the roller circumference is always homogeneously charged with one electron. In the "quasi-stochastic" regime, recharging of the stripe shifted counter clockwise by $\theta = \pi/6$ radians from the actually charged stripe is performed once its angle with the water surface drops below $\pi/6$ radians. In the "periodic" regime, recharging of the next counter clockwise positioned stripe is realized periodically every t_C, giving a charged wave on the surface.

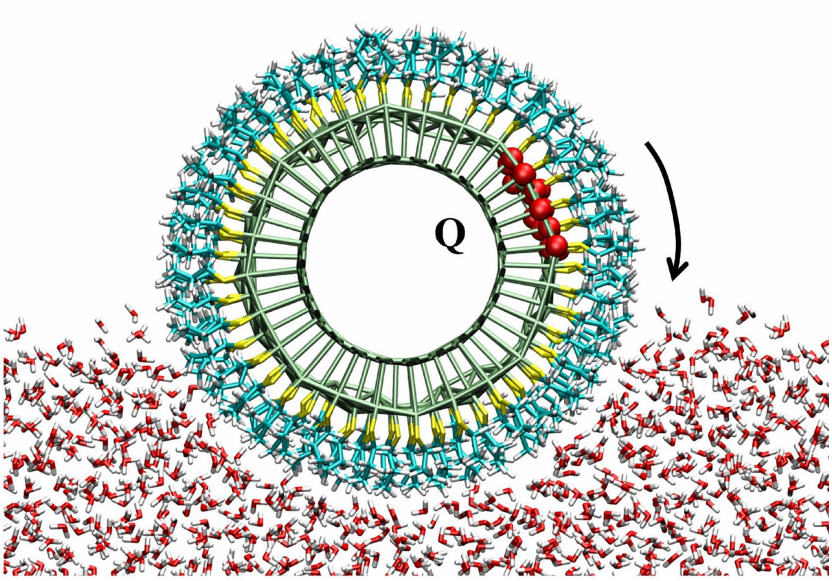

Figure 5. Model nanorod rolling on the water surface by Coulombically induced torque.

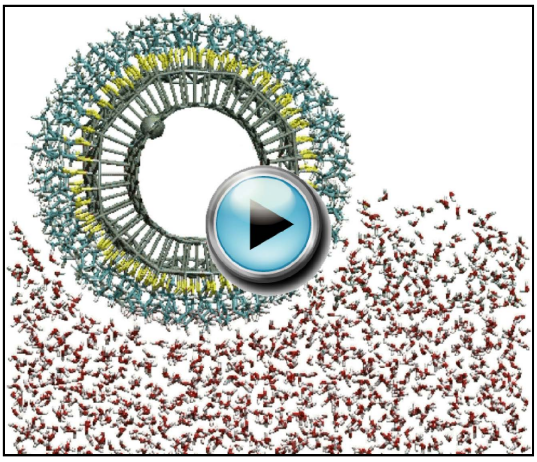

Movie 5. Rolling of nanorods on water by light

In reality, metallic nanorods can be covered with triblock surfactants, with the middle blocks made of partially oriented and photoactive chromophores, whereas inner and outer blocks could be inert and hydrophobic alkane chains. These nanorods could be rotated by excitation of their chromophores with a light beam tilted with respect to the water surface. Coulombic attraction of the transiently and asymmetrically polarized or charged chromophores in these nanorods to the polar water molecules should cause unidirectional reorientation (rolling) of the nanorods.

We have shown that with the proposed driving, nanorods with radii of $R_N = 2 - 5$ nm can roll on water with translational velocities of $v_{tran} = 1 - 5$ nm/ns [54]. The extent of coupling between rotational and translational motions is given by the efficiency of the rolling motion, defined as $S = v_{tran}/R_N\ v_{rot}$, where v_{rot} is the angular velocity. It turns out that translational velocities and efficiencies of the rolling motion depend on the coupling strength between surfactants and water, ε_s. While in the ideal (non-slipping) system, $S \rightarrow 1$, surfactant-covered nanorods roll on the dynamic water surface with greatly reduced efficiencies of $S = 0.1 - 0.4$. These simulations demonstrate that nanorods need to couple well to the water surface but not solvate in order to become propelled with minimal slipping during rotation [55].

Rotary Actuators in Nanofluidics

In order to control molecular flows in nanofluidics, novel synthetic nanopores might be also designed. Such pores could be based on principles similar to those operating in channel proteins. The protein cores are formed by precisely arranged sequences of amino acids that can efficiently recognize and guide the passing molecular species. Synthetic systems can have simpler structures, based on artificial proteins [55 – 58], coenzymes [59], and inorganic materials, such as zeolites [60], carbon [61] or silica [62]. Below, we describe recently explored molecular nanochannels, where rotary motion can control their selectivity and passage rates.

Molecular nanovalve

Previously, we have designed model hybrid nanochannels formed by covalently connected carbon nanocones [63]. In Figure 6 (left), we show two carbon nanocones that are stacked and connected by aliphatic chains at their open tips, in analogy to aquaporins. The functionality of this nanovalve structure is based on the fact that the size of the nanopore is altered when one nanocone is gradually rotated with respect to the other. If we mutually rotate them by a certain angle θ_{rot}, the aliphatic chains become stretched, helically wrapped, and entangled inside the nanopore. The rotation of nanocones is precise and reproducible, due to the π-π stacking.

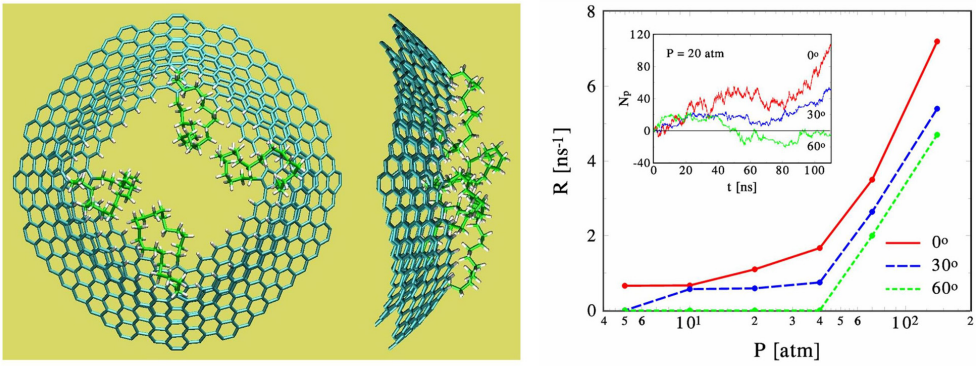

Figure 6. (left) The stacked (untwisted) pair of nanocones. (right) Dependence of the rate of pentane flow through the nanopore on the applied pressures, at rotation angles of $\theta_{rot} = 0^\circ$, 30° and 60°. (inset) The time dependence of total number of pentane molecules that pass the nanopore N_p, at the applied pressure of $P = 20$ atm and different θ_{rot}.

The size of the nanopore controls the flow of fluids through the nanovalve. In Figure 6 (right), we plot the dependence of the flow rates R on the pressure P at $\theta_{rot} = 0^\circ$, 30° and 60°. It turns out that R depends dramatically on both parameters. At $\theta_{rot} = 0^\circ$, the cone is opened and R is nonzero even at small pressures. At large pressures, R grows and is proportional to the pressure. At the angles where the cone is largely closed, $\theta_{rot} = 30^\circ$, 60°, the flow is almost zero at low pressures, $P < 10$ atm. At higher pressures, the cross section area of the nanopore can become slightly bigger for $\theta_{rot} = 30^\circ$, resulting in small constant flow in the region of $P = 10 - 40$ atm. At $P > 40$ atm, the four alkyl chains start to open for all the studied angles, and the flow increases with pressure.

In the inset of Figure 6 (right), we also show the time dependence of the total number of pentanes that pass the nanopore at $P = 20$ atm. The size of the time-dependent fluctuations in N_p reflects fluctuations in the sizes of the nanopore, caused by the alkyl chains that rotate and change their conformations. For more closed pores, the fluctuations of N_p are smaller, due to stretched alkyl chains.

Biomimetic ammonia switch

Nanochannels for selective molecular passage can be designed in direct analogy to channel proteins. Recently, we explored hybrid nanochannels with inorganic and polypeptide components by means of MD simulations [63]. In Figure 7 (left), we show a nanochannel formed by two carbon nanotubes joined by a cylindrical structure of antiparallel peptide chains. Rotation of one nanotube end with respect to the other results in either forward or backward-twisted peptide barrels in the middle of the nanochannel.

In Figure 7 (right), we present the hysteresis curve for the dependence of the twist angle on the torque applied to the parallel 8-residue structure. The results are obtained in one twisting trajectory going between the two end points (wrapped cylinders) and back, where each data point is averaged over 1,000 frames separated by 100 fs, after equilibration for 1 ns. The hysteresis curve shows that the structure can be stabilized in two configurations with non-zero twist angles, upon removal of the torque.

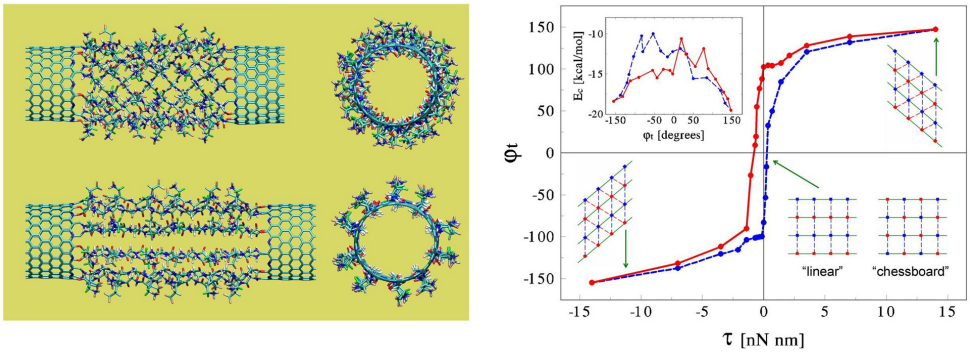

Figure 7. (left) Two types of 12-residue hybrid nanochannels solvated in water at T = 300 K. (right) The twist angle-torque hysteresis curve obtained in one cycle for the parallel 8-residue structure. Additional schemes show the charges and their mutual coupling in the straight and twisted structures. (inset) The related Coulombic energy-twist angle hysteresis curve.

These hybrid nanochannels are highly tunable due to a large selection of amino acids which can coat the inner channel walls. By screening the amino acid residues inside the peptide barrel, we identified those which make the channel interior selective to passage of ammonia. In Figure 8 (left), we show the interiors of this channel containing two tryptophan (TRP) and two tyrosine (TYR) residues for opposite twists, giving different internal structures. In Figure 8 (right), we plot the number N_p of NH_3 molecules passed under steady-state conditions through these channels within the simulation time t. The results show dramatically different flow rates, $R_{NH_3} = N_p/t$, for the forward and backward twisted configurations of the channel, $R^{for}_{NH_3} \approx 0.18\ ns^{-1}$, $R^{bac}_{NH_3} \approx 0$, respectively. In the forward twist, two pairs of interior residues shadow each other, thus increasing the cross section area available for the NH_3 passage. In the backward twist, the TRP and TYR residues are spread around the circumference of the channel, thus reducing the cross section area available for the NH_3 passage. These results strongly demonstrate that this highly tunable barrel junction can act as a mechanical switch for fluid flow.

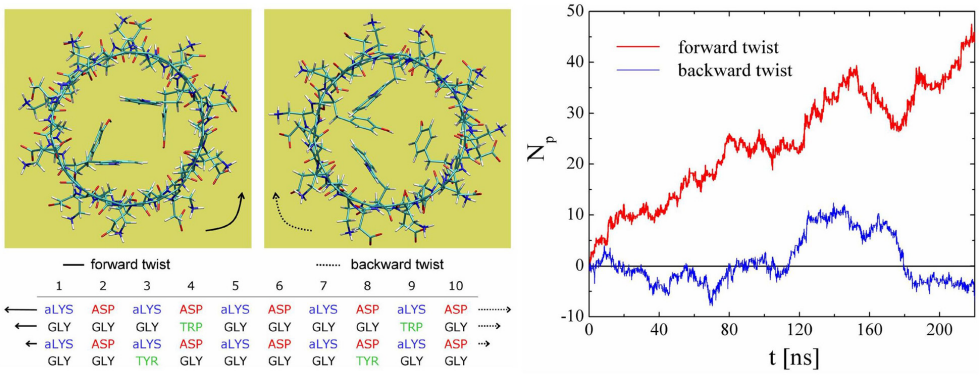

Figure 8. (left) Axial view of the two twisted configurations of the parallel 4-residue 10-peptide junction, with 2 tryptophan and 2 tyrosine residues in its interior. (left-bottom) Amino acid sequence map of 4-residue 10-peptide junction. Each column corresponds to a peptide chain, and the odd/even rows are residues with sidechains that are exposed outwards/inwards. (right) The time dependence of the total number N_p of NH_3 molecules passed through the twisted nanochannels.

Graphene nanopores

Selective molecular passage can also be realized in inorganic materials. For example, porous graphene monolayers can serve as membranes which selectively pass molecules without mechanical action. Recently, we modelled the passage of ions through functionalized nanopores in graphene monolayers by MD simulations [64]. In Figure 9, we display the studied pores with diameter of ≈ 5 Å, terminated by either negatively charged nitrogens and fluorines (left) or by positively charged hydrogens (right).

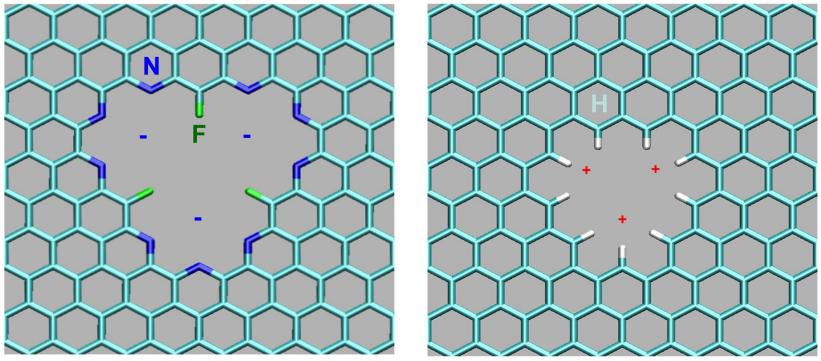

Figure 9. Functionalized graphene nanopores. (left) The F–N-terminated nanopore. (right) The H-terminated nanopore.

In Figure 10 (right insets), we show the configurations of the Na^+ and Cl^- ions passing through the two nanopores. The polar and charged nanopore rim can replace several water molecules from the first hydration shell of the ion passing through it. Therefore, the passing ion is surrounded by two separated first hydration "half-shells" at both sides. The close contact between the ion and the pore rim allows very efficient mapping and eventual removal of the ion shells, leading to the high selectivity of the ion passage.

Figure 10 (left insets) displays the time-dependent distance d between the ions and their pore centres, obtained at a low field of E = 6.25 mV/nm. The distance fluctuations reveal very different dynamics in two cases. The Na^+ ion passes the F–N-pore fast, without significantly binding with it. The ion rarely gets closer than 5 Å to the pore centre and stays most of the time in the water region (d > 10 Å). The ion passes through one of the three smaller holes in the nanopore with the C^3 symmetry. These asymmetric holes can not easily break the hydration shell of the Na^+ ion, which prohibits its prolonged stay in the pore. Simulations of K^+ ion show that its hydration shell can be more easily replaced by the pore rim upon shell partial removal, due to its weaker binding to the hydration shell.

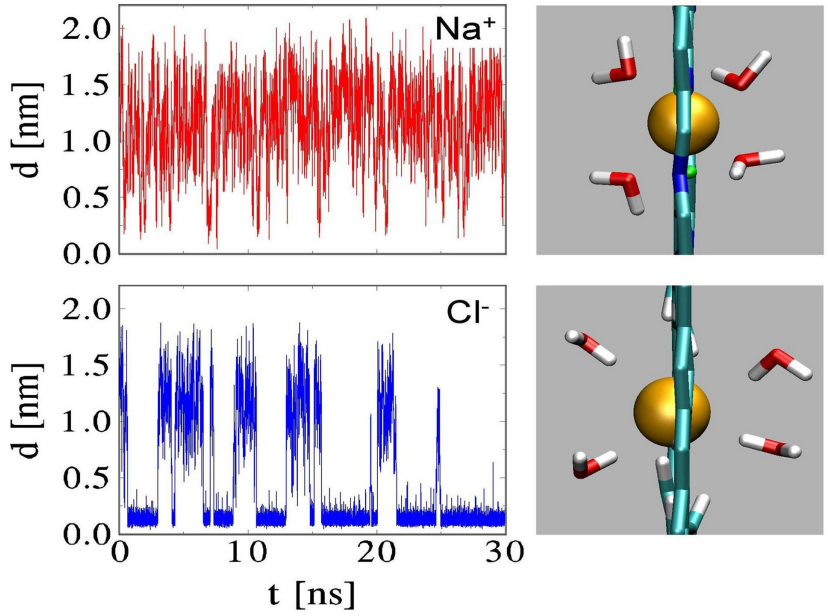

Figure 10. (left) Time-dependent distance d between the Na^+ and Cl^- ions and the centers of the F–N-pore and H-pore, respectively, at the field of E = 6.25 mV/nm. The dynamics of passage of these ions through the two pores is very different. (right) While both ions are surrounded by two water half-shells when passing through their pores, only the Cl^- ion has relatively stable binding to the H–pore.

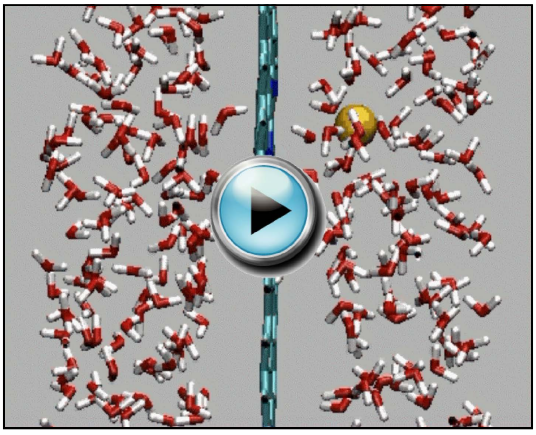

Movie 6. Passage of Na^+ ion through F-N-pore in graphene

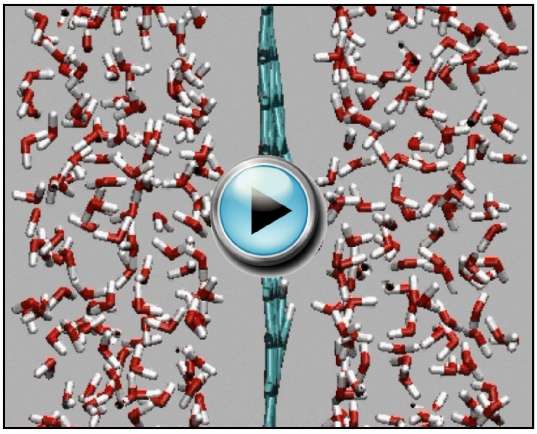

Movie 7. Passage of Cl^- ion through H-pore in graphene

The Cl^- ion has even more stable binding to the symmetric H-pore, where it stays for ≈ 70% of the time. At weak fields, the Cl^- ion enters and leaves the H-pore with almost the same rates from both sides. The electric field decreases the ion-pore binding, which is reflected in shorter time periods spent by the ion in the pore. At a field of E = 0.1 V/nm, the Cl^- ion stays in total only 30% of the time inside the pore. These and other recent theoretical and experimental studies [7, 65 – 67] indicate that porous graphene could serve as a sieve of high selectivity and transparency, and may be sensitive enough for applications including DNA sequencing.

Self-Assembly of Graphene-based Nanostructures

We may also try to control molecular motion during self-assembly into materials with unique shapes, interactions and properties. Carbon-based materials, including graphene, carbon nanotubes (CNTs), and their functionalized forms, can form such promising materials. Currently, graphene is intensively studied for its numerous potential applications [68 – 77]. For example, graphene nanoribbons (GNRs) have been synthesized [14, 78 – 80], and etched by using lithography [81, 82] and catalytic methods [83 – 85]. Graphene flakes with strong interlayer vdW coupling and chemical functionalization at their edges can self-assemble into larger structures [86 – 88]. Individual flakes with high elasticity [89 – 91] could fold into a variety of 3D structures [92], such as carbon nanoscrolls [93 – 96].

Droplet-driven self-assembly of graphene

Recently, we have studied how graphene stripes of different shapes can roll on themselves or around other structures (water droplets or CNTs) and form novel materials [97]. We have shown that water nanodroplets can induce rapid bending, folding, sliding, rolling, and zipping of planar nanostructures, which can lead to the assembly of nanoscale sandwiches, capsules, knots, and rings. In Figure 11 (top-left), we show that once a nanodroplet with $N_w = 1{,}300$ water molecules is placed at $T = 300$ K above a star-shaped flake, the droplet binds by vdW coupling to it and induces its bending and closing within $t \approx 1$ ns.

We have also shown that NDs can induce folding of graphene nanoribbons. As shown in Figure 11 (top right), when a ND ($N_w = 1{,}300$) is positioned above the free end of the ribbon (30×2 nm^2), the free end folds into a knot structure, touches the ribbon surface, and starts to slide fast on it due to strong vdW binding. When the radius of water droplet is several times bigger than the graphene width, it forms a multilayer ring structure, similar to multi-wall carbon nanotube, as seen in Figure 11 (bottom left). We have observed that GNRs can self-assemble into different nanostructures, and explored their dependence on the GNR width (w) and the water droplet radius (R_d). When $R_d > w$ the nanodroplet can activate and guide better the GNR assembly. The results are summarized in the phase diagram shown in Figure 11 (bottom right). Experimentally, the droplets could be deposited by Dip-Pen nanolithography [98] or AFM [99].

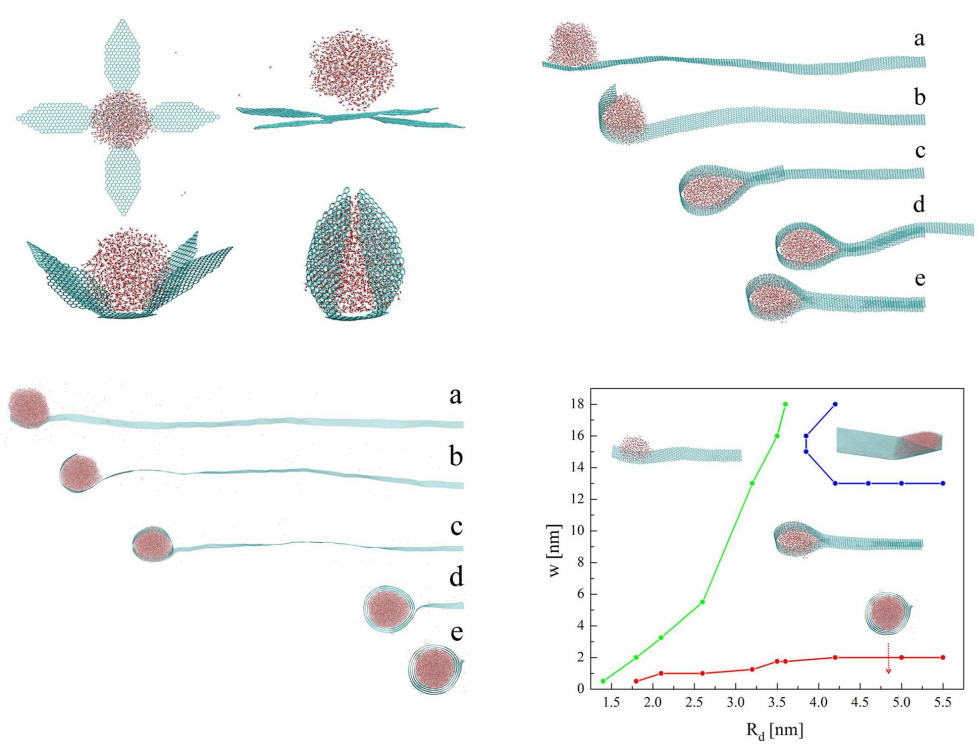

Figure 11. (top left) Nanodroplet-assisted folding of a star-shaped graphene flake. (top right) Folding and sliding of a graphene ribbon with the size of 30 × 2 nm^2, which is activated and guided by a nanodroplet with $N_w = 1{,}300$ waters and the radius of $R_d \approx 2.1$ nm. (bottom left) Folding and rolling of a graphene ribbon with the size of 90 × 2 nm^2, which is activated and guided by a nanodroplet with Nw = 10,000 waters and the radius of $R_d \approx 4.2$ nm. **(a-b)** The ribbon tip folds around the water droplet into a wrapped cylinder, and **(c-e)** the wrapped cylinder is induced to roll on the ribbon surface **(c-e)**. (bottom right) The phase diagram of graphene nanoribbon folding by water nanodroplets. We can see the nonfolding, sliding, rolling, and zipping phases.

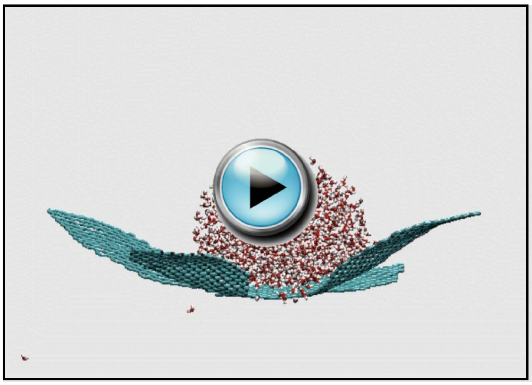

Movie 8. Self-assembly of graphene flake

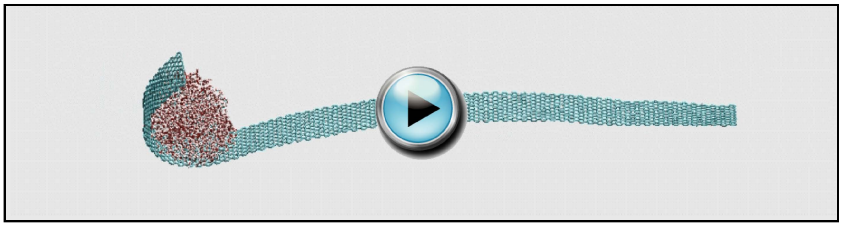

Movie 9. Sliding self-assembly of graphene stripe

Nanotube-driven self-assembly of graphene

We have also tested if CNTs and other nanoscale materials can activate and guide the self-assembly of GNRs on their surfaces and in their interiors [100]. In Figure 12, we present the results of our simulations of the CNT-assisted GNR self-assembly, sone at T = 300 K. Figure 12 (a-c) shows the self-assembly of the GNR (40 × 3 nm^2) once placed on the surface of (60,0) CNT (with two ends fixed). Figure 12 (d-e) shows the self-assembly of this GNR inside the same CNT. Figure 12 (f) shows that two GNRs (40 × 1 nm^2) can self-assemble into a double helix inside the same CNT. These results illustrate that GNR self-assembly can be activated and guided by CNTs.

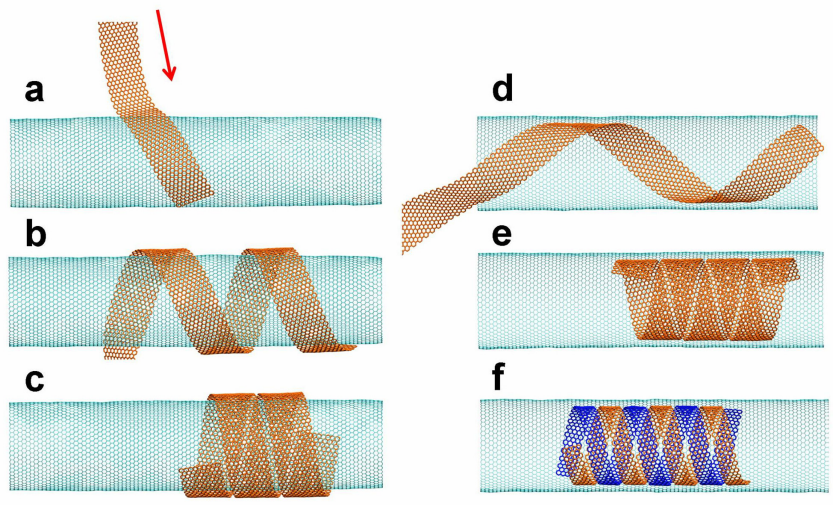

Figure 12. (a-c) Folding and rolling of a GNR with the size of 40 × 2 nm^2, when it is placed at the angle of 60° with respect to the axis of the (60,0) CNT. **(d-e)** Folding and rolling of this GNR when it is placed inside this CNT (front part of the CNT is removed for better visualisation). **(f)** Folding and rolling of two GNRs (40 × 1 nm^2) placed inside this CNT.

In the above described manner, one could in principle assemble arbitrary planar graphene nanostructures on the surfaces or in the interior of CNTs [101]. We test this idea on the self-assembly of a "hair-brush" like graphene nanostructure with four GNRs (60 × 2 nm^2). One end of all four GNRs is connected to the remaining part (40 × 100 nm^2) of the graphene sheet, and the distance between the adjacent GNRs is 5 nm, as shown in Figure 13 (a). Initially, the tips of all four GNRs are placed on the (20,0) CNT. They start to fold around it, and after t ≈ 4 ns, they form a single layer ring structures on the CNT. Within other t ≈ 3 ns, the GNRs make a multilayered ring structure. The rest of the graphene sheet also folds on the multilayered ring structures, and eventually completely wraps around the GNRs, as shown in Figure 13 (b-c). Then, we equilibrate the self-assembled structure, remove the CNT from its core, and equilibrate the remaining folded graphene. Upon removal, the diameter of the four rings slightly expands by 0.2 nm, as shown in Figure 13 (d-e), but the system retains the same shape, stabilized by the top graphene monolayer.

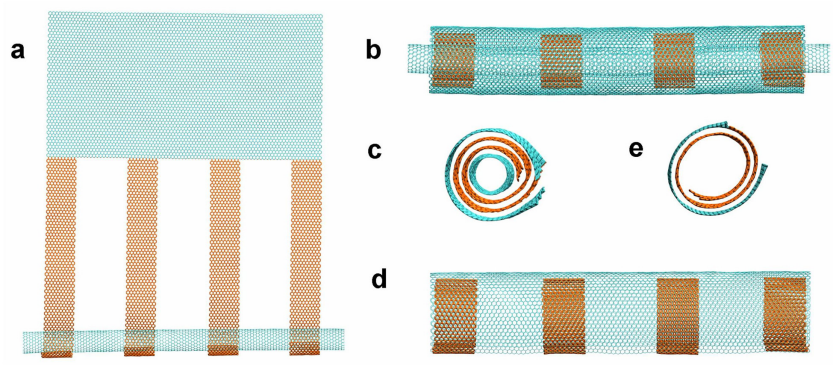

Figure 13. Graphene rings and knot formations from structured graphene flakes self-assembled on the CNT surface. **(a-c)** The formation of multiple GNR rings, covered with a single layer graphene sheet, on the (20,0) CNT. **(d-e)** After removal of the CNT, the multi-ring structure, covered with a single layer graphene sheet, is stabilized.

Conclusion

In summary, we have shown that control of rotary motion can be used in the preparation and activation of functional nanosystems. We discussed implementation of these principles in molecular propellers, motors, and rolling wheels. We have also shown how inorganic and biomimetic channels can be designed to serve as molecular switches, where mutual rotation of the individual components can control or selectively block the flow of different molecules. Finally, we have demonstrated that one could control the self-assembly of graphene nanostructures realized with the help of nanodroplets and graphene nanotubes. The studies can lead to the construction of building blocks in functional nanodevices, with unique mechanical, electrical, or optical properties, finding applications in electronics, sensing, and medicine.

References

[1] Bru, R., Sanchez-Ferrer, A. and Garcia-Carmona, F. (1995) Kinetic models in reverse micelles. *Biochem. J.* **310:**721 – 739.

[2] Valle, R. D. and Milligan, R.A. (2000) The way things move: looking under the hood of molecular motor proteins. *Science* **288:**88 – 95.
doi: 10.1126/science.288.5463.88.

[3] Gennerich, A. and Valle, R.D. (2009) Walking the walk: how kinesin and dynein coordinate their steps. *Curr. Opin. Cell Biol.* **21:**59 – 67 .
doi: 10.1016/j.ceb.2008.12.002.

[4] Bergs, J.S., Powell, B.C. and Cheney, R.E. (2001) A millenial myocin census. *Mol. Biol. Cell* **12:**780 – 794.

[5] Schliwa, M. (Ed.) Molecular Motors. 1st ed 2002. Wiley-VCH Weinheim, Germany.

[6] Atsumi, T., McCarter, L. and Imae, T. (1992) Polar and lateral flagellar motors of marine Vibrio are driven by different ion-motive forces. *Nature* **355**:182 – 184. doi: 10.1038/355182a0.

[7] van den Heuvel, M.G.L. and Dekker, C. (2007) Motor proteins at work for nanotechnology. *Science* **317:**333 – 336. doi: 10.1126/science.1139570.

[8] Soong, R.K., Bachand, G.D., Neves, H.P., Olkhovets, A.G., Craighead, H.G. and Montemagno, C.D. (2000) Powering an Inorganic Nanodevice with a Biomolecular Motor. *Science* **290:**1555 – 1558.

[9] Brunner, C., Wahnes, C. and Vogel, V. (2007) Cargo pick-up from engineered loading stations by kinesin driven molecular shuttles. *Lab on a Chip* **7**:1263. doi: 10.1039/b707301a.

[10] Goel, A. and Vogel, V. (2008) Harnessing biological motors to engineer systems for nanoscale transport and assembly. *Nat. Nanotechnol.* **3**:465 – 475. doi: 10.1038/nnano.2008.190.

[11] Green, J.E., Choi, J.W., Boukai, A., Bunimovich, Y., Johnston-Halperin, E., DeIonno, E., Luo, Y., Sheriff, B.A., Xu, K., Shin, Y.S., Tseng, H.-R., Stoddart, J.F. and Heath, J.R. (2007) A 160-kilobit molecular electronic memory patterned at 10^{11} bits per square centimeter. *Nature* **445:**414 – 417. doi: 10.1038/nature05462.

[12] Král, P. and Sadeghpour, H.R. (2002) Laser spinning of nanotubes: A path to fast-rotating microdevices. *Phys. Rev. B* **65**:161401 – 4(R). doi: 10.1103/PhysRevB.65.161401.

[13] Plewa, J., Tanner, E., Mueth, D.M. and Grier, D.G. (2004) Processing carbon nanotubes with holographic optical tweezers. *Opt. Express* **12:**1978 – 1981. doi: 10.1364/OPEX.12.001978.

[14] Tan, S., Lopez, H.A., Cai, C.W. and Zhang, Y. (2004) Optical Trapping of Single-Walled Carbon Nanotubes. *Nano Lett.* **4:**1415 – 1419. doi: 10.1021/nl049347g.

[15] Vacek, J. and Michl, J. (2001) Molecular dynamics of a grid-mounted molecular dipolar rotor in a rotating electric field. *Proc. Natl. Acad. Sci. U.S.A*. **98:**5481 – 5486. doi: 10.1073/pnas.091100598.

[16] Král, P. and Seideman, T. (2005) Current-induced rotation of helical molecular wires. *J. Chem. Phys.* **123:**184702 – 184706.
doi: 10.1063/1.2107527.

[17] Kelly, T.R., Silva, H. De and Silva, R.A. (1999) Unidirectional rotary motion in a molecular system. *Nature* **401:**150 – 152.
doi: 10.1038/43639.

[18] Barreiro, A., Rurali, R., Hernández, E.R., Moser, J., Pichler, T., Forro L. and Bachtold, A. (2008) Subnanometer motion of cargoes driven by thermal gradients along carbon nanotubes. *Science* **320:**775 – 778.
doi: 10.1126/science.1155559.

[19] Astumian, R.D. (1997) Thermodynamics and kinetics of a Brownian motor. *Science* **276:**917 – 922.
doi: 10.1126/science.276.5314.917.

[20] Bull, J.L., Hunt, A.J. and Meyhofer, E. (2005) A theoretical model of a molecular-motor-powered pump. *Biomed. Microdev.* **7:**21 – 33.
doi: 10.1007/s10544-005-6168-6.

[21] Andersson, H. and van den Berg, A. (2005) From lab-on-a-chip to lab-in-a-cell. *Proc. SPIE* 5718, 1.
doi: 10.1117/12.601553.

[22] Craighead, H.G. (2006) Future lab-on-a-chip technologies for interrogating individual molecules. *Nature* **442:**387 – 393.
doi: 10.1038/nature05061.

[23] Mannion, J.T. and Craighead, H.G. (2007) Nanofluidic structures for single biomolecule fluorescent detection. *Biopolymers* **85:**131 – 143.
doi: 10.1002/bip.20629.

[24] Kellermayer, M.S.Z. (2005) Visualizing and manipulating individual protein molecules. *Physiol. Meas.* **26:**R119-R153.
doi: 10.1088/0967-3334/26/4/R02.

[25] Strick,T., Allemand, J.-F., Croquette, V. and Bensimon, D. (2001) The manipulation of single biomolecules. *Physics Today* **54:**46 – 51.
doi: 10.1063/1.1420553.

[26] Ying, L. (2007) Single molecule biology: Coming of age. *Mol. BioSyst*. **3:**377 – 380.
doi: 10.1039/b702845 h.

[27] Iijima, S. (1991) Helical microtubules of graphitic carbon. *Nature* **354:**56 – 58.
doi: 10.1038/354056a0.

[28] Dresselhaus, M.S., Dresselhaus, G. and Eklund, P.C. (1996) Science of Fullerenes and Carbon Nanotubes. Academic Press Inc., San Diego.

[29] Novoselov, K.S., Geim, A.K., Morozov, S.V., Jiang, D., Zhang, Y., Dubonos, S.V., Grigorieva, I.V. and Firsov, A.A. (2004) Electric field effect in atomically thin carbon films. *Science* **306:**666 – 369.
doi: 10.1126/science.1102896.

[30] Zheng, M., Jagota, A., Strano, M.S., Santos, A.P., Barone, P., Chou, S.G., Diner, B.A., Dresselhaus, M.S., Mclean, R.S., Onoa, G.B., Samsonidze, G.G., Semke, E.D., Usrey, M. and Walls, D.J. (2003) Structure-based carbon nanotube sorting by sequence-dependent DNA assembly. *Science* **302:**1545 – 1548.
doi: 10.1126/science.1091911.

[31] Banerjee, S., Hemraj-Benny, T. and Wong, S.S. (2005) Covalent surface chemistry of single-walled carbon nanotubes. *Adv. Mater.* **17:**17 – 29.
doi: 10.1002/adma.200401340.

[32] Stankovich, S., Dikin, D.A., Dommett, G.H.B., Kohlhaas, K.M., Zimney, E.J., Stach, E.A., Piner, R.D., Nguyen, S.T. and Ruoff, R.S. (2006) Graphene-based composite material. *Nature* **442:**282 – 286.
doi: 10.1038/nature04969.

[33] Cervantes-Sodi, F., Csanyi, G., Piscanec, S. and Ferrari, A.C. (2008) Edge-functionalized and substitutionally doped graphene nanoribbons: Electronic and spin properties. *Phys. Rev. B* **77**: 165427 – 165439.
doi: 10.1103/PhysRevB.77.165427.

[34] Boukhvalov, D.W. and Katsnelson, M.I. (2008) Chemical functionalization of graphene with defects. *Nano Lett.* **8**:4373 – 4379.
doi: 10.1021/nl802234n.

[35] Ferro, S. and De Battisti, A. (2003) The 5-V window of polarizability of fluorinated diamond eletrodes in aqueous solutions. *Anal. Chem.* **75:**7040 – 7042.
doi: 10.1021/ac034717r.

[36] Dikin, D.A., Stankovich, S., Zimney, E.J., Piner, R.D., Dommett, G.H.B., Evmenenko, G., Nguyen S.T. and Ruoff, R.S. (2007) Preparation and characterization of graphene oxide paper. *Nature* **448:**457 – 460.
doi: 10.1038/nature06016.

[37] Cai, W., Piner, R.D., Stadermann, F.J., Park, S., Shaibat, M.A., Ishii, Y., Yang, D., Velamakanni, A., An, S.J., Stoller, M., An, J., Chen, D. and Ruoff, R.S. (2008) Synthesis and solid-state NMR structural characterization of 13C-labeled graphite oxide. *Science* **321:**1815 – 1817.
doi: 10.1126/science.1162369.

[38] Purcell, E.M. (1997) Life at low Reynolds number. *Amer. J. Phys.* **45:**1 – 3.

[39] Wang, B. and Král, P. (2007) Chemically tunable nanoscale propellers of liquids. *Phys. Rev. Lett.* **98**:266102 – 266105.
doi: 10.1103/PhysRevLett.98.266102.

[40] Han, J., Globus, A., Jaffe, R. and Deardorff, G. (1997) Molecular dynamics simulations of carbon nanotube-based gears. *Nanotechnology* **8:**95 – 102.
doi: 10.1088/0957-4484/8/3/001.

[41] Tasis, D., Tagmatarchis, N., Bianco, A. and M. Prato, (2006) Chemistry of Carbon Nanotubes. *Chem. Rev.* **106**:1105 – 1136.
doi: 10.1021/cr050569o.

[42] Silverstein, K.A.T., Haymet, A.D.J. and Dill, K.A. (2000) The Strength of Hydrogen Bonds in Liquid Water and Around Nonpolar Solutes. *J. Am. Chem. Soc.* **122**:8037 – 8041.
doi: 10.1021/ja000459t.

[43] Auinger, H. (2001) Efficiency of electric motors under practical conditions. *Power Eng. J.* **15**:163 – 167.
doi: 10.1049/pe:20010309.

[44] Park, H., Park, J., Lim, A.K.L., Anderson, E.H., Alivisatos, A.P. and McEuen, P.L. (2000) Nanomechanical oscillations in a single-C 60 transistor. *Nature* **407**:57 – 60.
doi: 10.1038/35024031.

[45] Kaun, C.C. and Seideman, T. (2005) Current-Driven Oscillations and Time-Dependent Transport in Nanojunctions. *Phys. Rev. Lett.* **94**:226801 – 226804.
doi: 10.1103/PhysRevLett.94.226801.

[46] Wang, B., Vuković L. and Král, P. (2008) Nanoscale rotary motors driven by electron tunneling. *Phys. Rev. Lett.* **101:**186808 – 186811.
doi: 10.1103/PhysRevLett.101.186808.

[47] Cumings, J. and Zettl, A. (2000) Low-Friction Nanoscale Linear Bearing Realized from Multiwall Carbon Nanotubes. *Science* **289:**602 – 604.
doi: 10.1126/science.289.5479.602.

[48] Cupas, C.A. and Hodakowski, L. (1974) Iceane. *J. Am. Chem. Soc*. **96:**4668 – 4669.
doi: 10.1021/ja00821a050.

[49] Mikkelsen, K.V. and Ratner, M.A. (1987) Electron tunnelling in solid-state electron-transfer reactions. *Chem. Rev.* **87:**113 – 153.
doi: 10.1021/cr00077a007.

[50] Král, P. (1997) Nonequilibrium linked cluster expansion for steady-state quantum transport. *Phys. Rev. B* **56:**7293 – 7303.
doi: 10.1103/PhysRevB.56.7293.

[51] Carella, A., Rapenne, G., Launay, J.-P. (2005) Design and synthesis of the active part of a potential molecular motor. *New J. Chem.* **29**:288 – 290.
doi: 10.1039/b415214j.

[52] Ashkin, A., Dziedzic, J.M., Bjorkholm, J.E. and Chu, S. (1986) Observation of a single-beam gradient force optical trap for dielectric particles. *Opt. Lett*. **11:**288 – 290.
doi: 10.1364/OL.11.000288.

[53] Holmlin, R.E., Schiavoni, M., Chen, C.Y., Smith, S.P., Prentiss, M.G. and Whitesides, G.M. (2000) Light-Driven Microfabrication: Assembly of Multicomponent, 3D Structures Using Optical Tweezers. *Angew. Chem. Int. Ed. Engl.* **39:**3503 – 3506.
doi: 10.1002/1521-3773(20001002)39:19<3503::AID-ANIE3503>3.0.CO;2-M.

[54] Vuković, L. and Král, P. (2009) Coulombically Driven Rolling of Nanorods on Water. *Phys. Rev. Lett.* **103:**246103 – 246106.
doi: 10.1103/PhysRevLett.103.246103.

[55] Qi, Z., Sokabe, M., Donowaki, K. and Ishida, H. (1999) Structure-Function Study on a de Novo Synthetic Hydrophobic Ion Channel. *Biophys. J.* **76:**631 – 641.
doi: 10.1016/S0006-3495(99)77231-0.

[56] Kuhlman, B., Dantas, G., Ireton, G.C., Varani, G., Stoddard, B.L. and Baker, D. (2003) Design of a Novel Globular Protein Fold with Atomic-Level Accuracy. *Science*, **302:**1364 – 1368.
doi: 10.1126/science.1089427.

[57] Kaplan, J. and DeGrado, W.F. (2004) De novo design of catalytic proteins. *Proc. Natl. Acad. Sci. U.S.A*. **101:** 1566 – 11570.
doi: 10.1073/pnas.0404387101.

[58] Tsai, C.-J., Zheng, J. and Nussinov, R. (2006) Designing a Nanotube Using Naturally Occurring Protein Building Blocks. *PLoS Comput. Biol*. **2:**e42.
doi: 10.1371/journal.pcbi.0020042.

[59] Murakami, Y., Kikuchi, J., Hisaeda, Y. and Hayashida, O. (1996) Artificial Enzymes. *Chem. Rev.* **96:**721 – 758.
doi: 10.1021/cr9403704.

[60] Jordan, E., Bell, R.G., Wilmer, D. and Koller, H. (2006) Anion-Promoted Cation Motion and Conduction in Zeolites. *J. Am. Chem. Soc*.**128:** 558 – 567.
doi: 10.1021/ja0551887.

[61] Saufi, S.M. and Ismail, A.F. (2004) Fabrication of carbon membranes for gas separationa review. *Carbon* **42:**241 – 259.
doi: 10.1016/j.carbon.2003.10.022.

[62] Duke, M.C., da Costa, J.C.D., Do, D.D.; Gray, P.G. and Lu, G.Q. (2006) Hydrothermally Robust Molecular Sieve Silica for Wet Gas Separation. *Adv. Funct. Mater.* **16:**1215 – 1220.
doi: 10.1002/adfm.200500456.

[63] Titov, A.V., Wang, B., Sint, K. and Král, P. (2010) Controllable Synthetic Molecular Channels: Biomimetic Ammonia Switch. *J. Phys. Chem. B*, **114:**1174 – 1179.
doi: 10.1021/jp9103933.

[64] Sint, K., Wang, B. and Král, P. (2008) Selective Ion Passage through Functionalized Graphene Nanopores. *J. Am. Chem. Soc.* **130:**16448 – 16449.
doi: 10.1021/ja804409f.

[65] Garaj, S., Hubbard, W., Reina, A., Kong, J., Branton, D. and Golovchenko, J.A. (2010) Graphene as a subnanometre trans-electrode membrane. *Nature* **467:**190 – 193.
doi: 10.1038/nature09379.

[66] Merchant, C.A., Healy, K., Wanunu, M., Ray, V., Peterman, N., Bartel, J., Fischbein, M.D., Venta, K., Luo, Z., Johnson, A.T.C, and Drndić, M. (2010) DNA Translocation through Graphene Nanopores. *Nano Lett.* **10:**2915 – 2921.
doi: 10.1021/nl101046t.

[67] Nelson, T., Zhang, B. and Prezhdo, O.V. (2010) Detection of Nucleic Acids with Graphene Nanopores: Ab Initio Characterization of a Novel Sequencing Device. *Nano Lett.* **10:**3237 – 3242.
doi: 10.1021/nl9035934.

[68] Novoselov, K.S., Geim, A.K., Morozov, S.V., Jiang, D., Zhang, Y., Dubonos, S.V., Grigorieva, I.V. and Firsov, A.A. (2004) Electric Field Effect in Atomically Thin Carbon Films. *Science* **306:**666 – 669.
doi: 10.1126/science.1102896.

[69] Geim, A.K. and Novoselov, K.S. (2007) The rise of graphene. *Nat. Mater.* **6:**183 – 191.
doi: 10.1038/nmat1849.

[70] Berner, S., Corso, M., Widmer, R., Groening, O., Laskowski, R., Blaha, P., Schwarz, K., Goriachko, A., Over, H., Gsell, S., Schreck, M., Sachdev, H., Greber, T. and Osterwalder, J. (2007) Boron Nitride Nanomesh: Functionality from a Corrugated Monolayer. *Angew. Chem. Int. Ed.* **46:**5115 – 5119.
doi: 10.1002/anie.200700234.

[71] Laskowski, R., Blaha, P., Gallauner, T. and Schwarz, K. (2007) Single-Layer Model of the Hexagonal Boron Nitride Nanomesh on the Rh(111) Surface. *Phys. Rev. Lett.* **98:**106802 – 106805.
doi: 10.1103/PhysRevLett.98.106802.

[72] Tsoukleri, G., Parthenios, J., Papagelis, K., Jalil, R., Ferrari, A. C., Geim, A.K., Novoselov, K.S. and Galiotis, C. (2009) Subjecting a Graphene Monolayer to Tension and Compression. *Small* **5:**2397 – 2402.
doi: 10.1002/smll.200900802.

[73] Balog, R., Jorgensen, B., Nilsson, L., Andersen, M., Rienks, E., Bianchi, M., Fanetti, M., Laegsgaard, E., Baraldi, A., Lizzit, S., Sljivancanin, Z., Besenbacher, F., Hammer, B., Pedersen, T.G., Hofmann, P. and Hornekaer, L. (2010) Bandgap opening in graphene induced by patterned hydrogen adsorption. *Nat. Mater.* **9:**315 – 319.
doi: 10.1038/nmat2710.

[74] Yan, X., Cui, X., Li, B. and Li, L.-s. (2010) Large Solution-Processable Graphene Quantum Dots as Light Absorbers for Photovoltaics. *Nano Lett.* **10:**1869 – 1873.
doi: 10.1021/nl101060 h.

[75] Cohen-Karni, T., Qing, Q., Li, Q., Fang, Y. and Lieber, C. M. (2010) Graphene and Nanowire Transistors for Cellular Interfaces and Electrical Recording. *Nano Lett.* **10:**1098 – 1102.
doi: 10.1021/nl1002608.

[76] Wang, Y., Shao, Y., Matson, D.W., Li, J. and Lin, Y. (2010) Nitrogen-Doped Graphene and Its Application in Electrochemical Biosensing. *ACS Nano* **4:**1790 – 1798.
doi: 10.1021/nn100315s.

[77] Matyba, P., Yamaguchi, H., Eda, G., Chhowalla, M., Edman, L. and Robinson, N. D. (2010) Graphene and Mobile Ions: The Key to All-Plastic, Solution-Processed Light-Emitting Devices. *ACS Nano* **4:**637 – 642.
doi: 10.1021/nn9018569.

[78] Jiao, L., Zhang, L., Wang, X., Diankov, G. and Dai, H. (2009) Narrow graphene nanoribbons from carbon nanotubes. *Nature* **458:**877 – 880.
doi: 10.1038/nature07919.

[79] Shi Kam, N.W., Jessop, T.C., Wender, P.A. and Dai, H. (2004) Nanotube Molecular Transporters: Internalization of Carbon Nanotube-Protein Conjugates into Mammalian Cells. *J. Am. Chem. Soc*. **126:**6850 – 6851.
doi: 10.1021/ja0486059.

[80] Kosynkin, D.V., Higginbotham, A.L., Sinitskii, A., Lomeda, J.R., Dimiev, A., Price, B.K. and Tour, J.M. (2009) Longitudinal unzipping of carbon nanotubes to form graphene nanoribbons. *Nature* **458:**872 – 876.
doi: 10.1038/nature07872.

[81] Tapaszto, L., Dobrik, G., Lambin, P. and Biro, L.P. (2008) Tailoring the atomic structure of graphene nanoribbons by scanning tunnelling microscope lithography. *Nat. Nanotechnol.* **3:**397 – 401.
doi: 10.1038/nnano.2008.149.

[82] Stampfer, C., Gttinger, J., Hellmller, S., Molitor, F., Ensslin, K. and Ihn, T. (2009) Energy Gaps in Etched Graphene Nanoribbons. *Phys. Rev. Lett.* **102:**056403 – 056407.
doi: 10.1103/PhysRevLett.102.056403.

[83] Ci, L., Xu, Z., Wang, L., Gao, W., Ding, F., Kelly, K.F., Yakobson, B.I. and Ajayan, P.M. (2008) Controlled nanocutting of graphene. *Nano Res*. **1:**116 – 122.
doi: 10.1007/s12274-008-8020-9.

[84] Campos, L.C., Manfrinato, V.R., Sanchez-Yamagishi, J.D., Kong, J. and Jarillo-Herrero, P. (2009) Anisotropic Etching and Nanoribbon Formation in Single-Layer. *Nano Lett*. **9:**2600 – 2604.
doi: 10.1021/nl900811r.

[85] Kim, K., Sussman, A. and Zettl, A. (2010) Graphene Nanoribbons Obtained by Electrically Unwrapping Carbon Nanotubes. *ACS Nano* **4:**1362 – 1366.
doi: 10.1021/nn901782g

[86] Zhu, Z., Su, D., Weinberg, G. and Schlogl, R. (2004) Supermolecular Self-Assembly of Graphene Sheets: Formation of Tube-in-Tube Nanostructures. *Nano Lett.* **4:**2255 – 2259.
doi: 10.1021/nl048794t.

[87] Jin, W., Fukushima, T., Niki, M., Kosaka, A., Ishii, N. and Aida, T. (2005) Self-assembled graphitic nanotubes with one-handed helical arrays of a chiral amphiphilic molecular graphene. *Proc. Natl. Acad. Sci. U.S.A*. **102:**10801 – 10806.
doi: 10.1073/pnas.0500852102.

[88] Chen, Q., Chen, T., Pan, G.-B., Yan, H.-J., Song, W.-G., Wan, L.-J., Li, Z.-T., Wang, Z.-H., Shang, B., Yuan, L.-F. and Yang, J.-L. (2008) Structural selection of graphene supramolecular assembly oriented by molecular conformation and alkyl chain. *Proc. Natl. Acad. Sci. U.S.A.* **105:**16849 – 16854.
doi: 10.1073/pnas.0809427105.

[89] Lee, C., Wei, X., Kysar, J. W. and Hone, J. (2008) Measurement of the Elastic Properties and Intrinsic Strength of Monolayer Graphene. *Science* **321:**385 – 388. doi: 10.1126/science.1157996.

[90] Bunch, J.S., Verbridge, S.S., Alden, J. S., van der Zande, A.M., Parpia, J.M. Craighead, H.G. and McEuen, P.L. (2008) Impermeable Atomic Membranes from Graphene Sheets. *Nano Lett*. **8:**2458 – 2462. doi: 10.1021/nl801457b.

[91] Gomez-Navarro, C., Burghard, M. and Kern, K. (2008) Elastic Properties of Chemically Derived Single Graphene Sheets. *Nano Lett*. **8:**2045 – 2049. doi: 10.1021/nl801384y.

[92] Bets, K.V. and Yakobson, B I. (2009) Spontaneous Twist and Intrinsic Instabilities of Pristine Graphene Nanoribbons. *Nano Res*. **2:**161 – 166.

[93] Viculis, L.M., Mack, J.J. and Kaner, R.B. (2003) A Chemical Route to Carbon Nanoscrolls. *Science* **299:**1361 – 1361. doi: 10.1126/science.1078842.

[94] Braga, S.F., Coluci, V.R., Legoas, S.B., Giro, R., Galvao, D.S. and Baughman, R. H. (2004) Structure and Dynamics of Carbon Nanoscrolls. *Nano Lett*. **4:**881 – 884. doi: 10.1021/nl0497272.

[95] Yu, D. and Liu, F. (2007) Synthesis of Carbon Nanotubes by Rolling up Patterned Graphene Nanoribbons Using Selective Atomic Adsorption. *Nano Lett*. **7:**3046 – 3050. doi: 10.1021/nl071511n.

[96] Sidorov, A., Mudd, D., Sumanasekera, G., Ouseph, P.J., Jayanthi, C.S. and Wu, S.-Y. (2009) Electrostatic deposition of graphene in a gaseous environment: a deterministic route for synthesizing rolled graphenes? *Nanotechnology* **20:**055611 – 055615. doi: 10.1088/0957-4484/20/5/055611.

[97] Patra, N., Wang, B. and Král, P. (2009) Nanodroplet Activated and Guided Folding of Graphene Nanostructures. *Nano Lett*. **9:**3766 – 3771. doi: 10.1021/nl9019616.

[98] Lee, K.-B., Park, S.-J., Mirkin, C.A., Smith, J.C. and Mrksich, M. (2002) Protein Nanoarrays Generated By Dip-Pen Nanolithography. *Science* **295:**1702 – 1705. doi: 10.1126/science.1067172.

[99] Duwez, A.-S., Cuenot, S., Jerome, C., Gabriel, S., Jerome, R., Rapino, S. and Zerbetto, F. (2006) Mechanochemistry: targeted delivery of single molecules. *Nat. Nanotechnol*. **1:**122 – 125. doi: 10.1038/nnano.2006.92.

[100] Patra, N., Song, Y. and Král, P. (2010) Self-assembly of Graphene Nanostructures on Nanotubes. *ACS Nano*. Online February 22, 2011.